Acta Technica *62* (2017), No. 7A, 439–450

Design of vibration intelligent detector based on temperature compensation technology

Han Lv[1,2], Peng Wu[1,*]

Abstract. A fiber optic vibration measurement system with temperature compensation function is designed with respect to the issue that fiber vibration sensor is sensitive to temperature and has low sensitivity. The system establishes two complementary and systematic sensing channels by using the transmission-type matching FBG with its center wavelength systematically located on both sides of the fiber Bragg grating (FBG). The vibration sensing is realized with the difference principle. This paper analyzes and tests the effect of the simultaneous measurement of vibration and temperature. The results show that vibration has little impact on FBG center wavelength. Data processing enables the elimination of the effect of F-P filter scanning on vibration measurement.

Key words. Temperature compensation, Vibration detection, Fiber sensor, Fiber Bragg grating.

1. Introduction

The monitoring of vibration in civil infrastructure or industrial equipment enables disaster warning and health diagnosis, which is of vital significance. The fiber vibration sensor outweigh traditional vibration sensor for its resistance to electromagnetic interference, small size and reusability and has been widely applied to civil engineering, petrochemical and power system fields.

The fiber vibration acceleration sensor mainly includes wavelength modulation, phase modulation, polarization state and intensity modulation types when classified by the principle of sensing. The wavelength modulation sensor provides low noise. Sensors of phase and polarization state types have higher demodulation sensitivity. The intensity modulation sensor is simpler in its demodulation principle.

[1]Institute of Seismology, CEA, Wuhan, China, 430071
[2]Wuhan Research Institute of Seismologic Instruments, Wuhan, China, 430071
*. Corresponding author

These sensors present the issues of complex encapsulation structure and sensitivity to temperature. The metal vibratory gyro is equipped with core resonator made of flexible alloy. It offers relatively simple processing technology, high yield and is easy to implement. However, metal material itself has higher coefficient of temperature and thermal expansion and is highly sensitive to temperature changes. Such temperature change heavily affects the random drift and zero position output of gyro. It is therefore that stable control of and normal compensation for ambient temperature will significantly improve gyro precision. If the temperature control system is used to keep gyro running at constant temperature, it will significantly improve gyro precision; however, there will also a big increase in the costs, energy consumption and volume of the device. On this occasion, the temperature compensation algorithm will offer a significant advantage in greatly improving gyro precision and posing little impact on cost, energy consumption and volume.

This paper makes improvement for sensor structure and designs a demodulation system for simultaneous measurement of vibration and ambient temperature in order to minimize the effect of temperature on sensor and improve sensor sensitivity. The vibration measurement is compensated by ambient temperature for purpose of minimizing the effect of temperature on the vibration sensing property.

2. Structural design

2.1. Traditional metal vibratory gyro

The metal vibration gyro is a new solid vibratory gyro that consists of a resonator, a piezoelectric electrode, a base and a cover, as shown in Fig. 1. The resonator is a sensitive flexible element securely fixed to the based with screws and is placed in the cover. It is generally required to supply vacuum to the cover where the disturbance on the resonator will be minimized in order to stabilize vibration. The basic operating principle of the metal vibratory gyro is that the cup-like resonator generates standing-wave vibration in the resonance state; when the resonator rotates at the angular rate, the standing-wave vibration will make precessional motion relative to the resonator in the presence of Coriolis force, and the rate of precession in vibration mode of standing-wave vibration will be directly proportional to the input angular rate.

Due to the fact that the header system is encapsulated in vacuum, and the installation of temperature sensor is only allowed on the housing, the temperature gradient is higher under vacuum condition. Therefore, the temperature of housing will not fully correspond to that of the resonator itself. In particular, it cannot reflect additional temperature changes of resonator arising out of heating due to vibration. The temperature compensation option based on temperature sensor often offers low precision and poor vibration detection result.

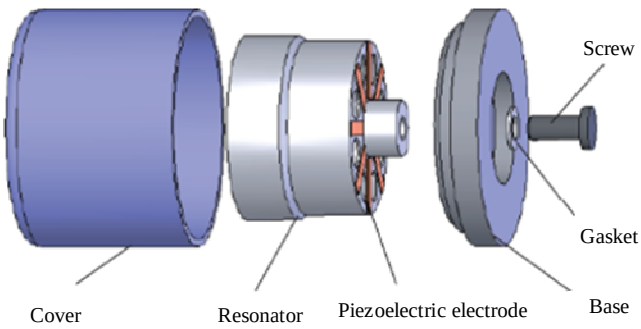

Fig. 1. Components of metal vibratory gyro

2.2. Principle of fiber optic vibration sensing

FBG is encapsulated in the form of stick-on beam for purpose of protection. Upon encapsulation, the relative motion of its Brace wavelength subject to strain and temperature may be expressed in:

$$\Delta\lambda_B/\lambda_B = (1-p_e)\,\varepsilon + [\alpha_s + \xi_s + (1-p_e)\,(\alpha_{s1} - \alpha_s)]\,\Delta t\,. \tag{1}$$

Where, λ_B and $\Delta\lambda_B$ are Bragg wavelength in the presence of strain and temperature and the wavelength shift in the presence of strain and temperature, respectively, in mm; α_s is the coefficient of thermal expansion of fiber optic; ξ_s is thermo-optical coefficient; α_{s1} is the coefficient of linear expansion of the encapsulator. For common silicon-base fiber, $\alpha_s \approx 0.5 \times 10^{-6}/^{\circ}\mathrm{C}$, $\xi_s \approx 7 \times 10^{-6}/^{\circ}\mathrm{C}$, and the coefficient of linear expansion of the encapsulator α_{s1} depends on the beam material used; ε is the axial strain of FAG as a result of strain; p_e is the valid elastic-optic constant of fiber optic. p_e of the common silicon-base fiber is approximately 0.22. To compensate for the effect of temperature in the said formula, 2 FBGs with similar wavelength are stuck to two beams with identical material and shape.

The beam stuck with grating λ_1 and the beam stuck grating λ_2 are hinged at both ends of X. The force analysis shows that in the case of neglecting slight deformation of both beams, the X frame will split the force equally on both beams when the beam with grating λ_1 is subject to tension F; however, the force on the other beam is pressure. The wavelength changes of two FBGs are:

$$\Delta\lambda_1/\lambda_1 = (1-p_e)\,\varepsilon_1 + [\alpha_s + \xi_s + (1-p_e)\,(\alpha_{s1} - \alpha_s)]\,\Delta t\,, \tag{2}$$

$$\Delta\lambda_2/\lambda_2 = (1-p_e)\,\varepsilon_y + [\alpha_s + \xi_s + (1-p_e)\,(\alpha_{s1} - \alpha_s)]\,\Delta t\,. \tag{3}$$

In formulas (2) and (3), ε_1 and ε_y are the tensile strain and compressive strain of beams in the presence of force F, respectively. $\Delta\lambda_1$ is positive and $\Delta\lambda_2$ is negative. Two beams have identical stress-strain and temperature properties as they share the same material and shape. It is designed that λ_2 is slightly greater than λ_1,

$\lambda_2 - \lambda_1 = \Delta\lambda_0$, and is approximate to $\lambda_2 = \lambda_1 = \lambda$. The reflection peak interval of two FAGs decreases in the presence of tensile force F, and the variation of peak interval is: $\lambda\left[(1-p_e)\,\varepsilon_1 + (1-p_e)\,\varepsilon_y\right]$. Therefore, the reflection peak spacing of the two FHGs is:

$$\Delta\lambda = \Delta\lambda_0 - \lambda\left[(1-p_e)\,\varepsilon_1 + (1-p_e)\,\varepsilon_y\right] \tag{4}$$

It shows that the variation of the peak interval and the two reflection peaks are independent of the temperature, and the sensitivity of the force and the strain are doubled. When force F has a periodic jitter on a constant basis, the two FAGs should be superimposed with new jitter strain, in which case, the reflection peak interval is:

$$\Delta\lambda = \Delta\lambda_0 - \lambda\left[(1-p_e)\left(\varepsilon_1 + \Delta\varepsilon_1\cos\omega t\right) + (1-p_e)\left(\varepsilon_y + \Delta\varepsilon_y\cos\omega t\right)\right]. \tag{5}$$

Where, the tensile strain and the compressive strain are composed of two terms: one is the constant strain preset by the constant force and the other is the jitter strain superimposed. With $\Delta\lambda$, demodulation of the strains independent of temperature will be possible. Matching of two FAGs with filter may demodulate the vibration information.

3. Fiber sensor and its demodulation system

3.1. Structure and operating principle of fiber sensor

The mechanical structure of the sensor consists of a cantilever, a substrate and a fixed plate, as shown in Fig. 2. The single mode fiber in the sensor is engraved with a fiber Bragg grating (FBG). The fiber part with grating region is stuck to one side of the cantilever, and the part without grating region is squeezed between the substrate and the cantilever. When vibrations are applied to the sensor, the cantilever periodically presses the single mode fiber to make a slight deformation of the fiber. Fiber deformation will turn part of the transmission modes in optic fiber to radiation mode, resulting in the radiation of part of the incident and the reflection light transmitted in the fiber core to fiber cladding. The light eventually loses so that optical power in the optical fiber is modulated by vibration. The demodulation of the changes in the optical power detected by the system enables the measurement of vibration acceleration, while the FBG mounted on the substrate measures the temperature of the environment where the sensor is.

3.2. Operating principle of demodulation system

The demodulation system converts the change in optical power arising out of vibration into the change in output voltage. It demodulates the change in FBG center wavelength. The structure diagram of the demodulation system is shown in Fig. 3. The light from the broadband light source enters the optical fiber sensor through the circulator, and enters the tunable F-P filter via FBG after intensity modulation. The 3 dB bandwidth of the transmission spectrum for the tunable

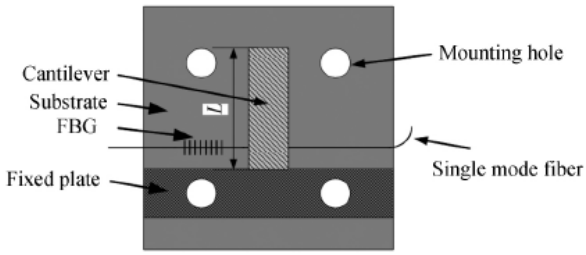

(a) Top view of sensor

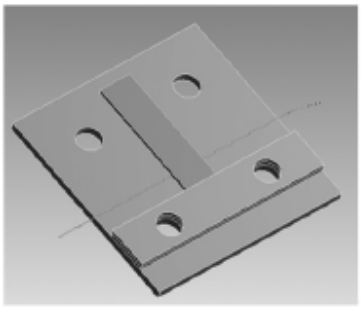

(b) Three-dimensional view of sensor

Fig. 2. Structure of fiber sensor

F-P filter used by the system is 0.177nm, and the free spectrum range (FSR) is 98.8nm, with the precision of 574. Fig. 4 shows the reflection spectrum of the tunable FP filter at the constant scanning voltage. It can be seen that when the wideband light enters the tunable FP filter, only a fraction of the light with a narrow bandwidth is transmitted through and most of the light is reflected. The reflection light enters photodetector 1 through the circulator and acquires data via channel 1 of data acquisition card. On this account, the voltage value acquired by channel 1 is linearly correlated to the vibration acceleration, which will realize the measurement of vibration acceleration. This design will improve the sensitivity of vibration measurement as the reflectivity of the tunable FP filter is much higher than the one of the fiber end face.

The tunable F-P filter scans the transmitted light of FBG in a triangular wave drive. The scanned light is split into two parts by the coupler, part of which directly enters photodetector 2 and is converted to voltage signal, and the other part enters F-P etalon via the isolator. Fig. 5(a) shows the transmission spectrum of the FBG obtained by channel 2 of the data acquisition card. The negative peak is formed when the FBG filters out the light with the same wavelength as the center wavelength of the broadband light source. Fig. 5 (b) is the transmission spectrum developed by F-P etalon; there is a negative peak in the spectrum because the F-P etalon used in the system has the wavelength labeling function. On the left side of the negative peak is a positive peak with smaller amplitude that corresponds to the negative peak as shown in Fig. 5 (a). This is also a result of FBG activity. With the transmission peak of F-P etalon as shown in Fig. 5 (b) FP as a reference, FBG center wavelength

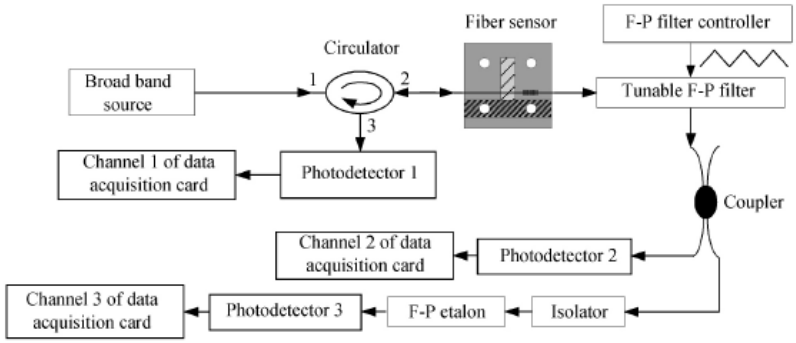

Fig. 3. Structure diagram of demodulation system

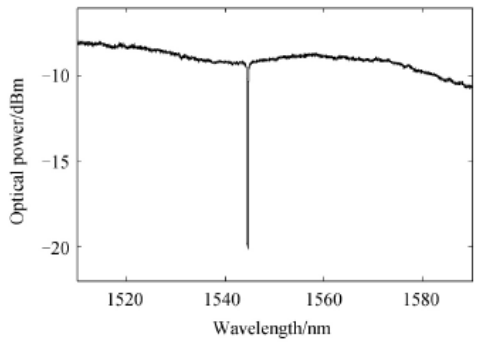

Fig. 4. Reflection spectrum of tunable F-P filter

may be demodulated, which means that the measurement of temperature is possible. The mechanical structure of both FBG and the sensor lies in the same temperature condition. It is possible to correct the vibration acceleration with the temperature measured by FBG so to as achieve temperature compensation.

4. Experimental analysis

4.1. Experimental apparatus

In the FBG vibration demodulation system shown in Fig. 1, FBG of same batch from Technica SA is used to keep consistency of FBG parameters used in the experiment. After experimental calibration, FBG has a temperature coefficient of 12 pm/°C and a center wavelength of 1 546.85 nm as sealed at 25°, in which center wavelength of FBG1 and FBG2 is 1546.79 nm and 1546.91nm respectively. In the system, FBG vibration sensor has a structure of cantilever beam with equal strength. The diagram of vibration sensor experimental system is shown in Fig. 6.

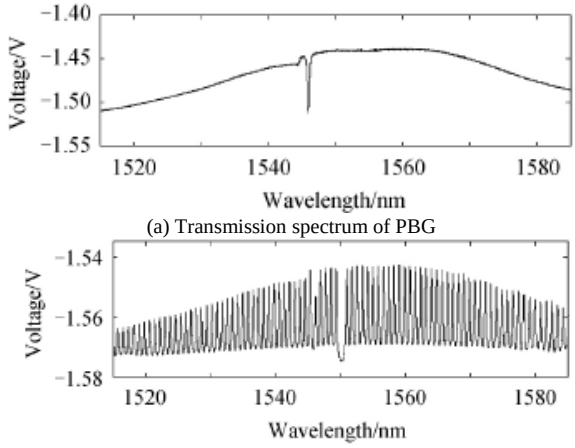

Fig. 5. Transmission spectra of F-P etalon and FBG

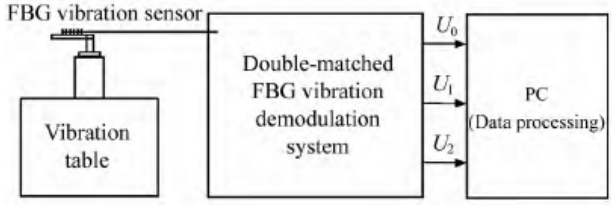

Fig. 6. Schematic diagram of the vibration demodulation system

4.2. Experiment Analysis

During experiment, place the vibration sensor in thermostatic bath and set the control circuit of TEC to achieve FBG fitting temperature of 30°C, meanwhile, make$\lambda_{B_1} = 1546.85$nm, $\lambda_{B_2} = 1546.97$nm, regulate the temperature of thermostatic bath from 20° to 40°, record U_0 and U_1 upon each change of 1°, use formula (1) and (8) to obtain the normalized output voltage U of demodulation channel and temperature compensation to determine the normalized output voltage U' of the channel. Results are shown in Fig. 7 and 8, in which the value of λ_s is calculated with temperature.

In Fig. 7, the long and thin curve means the experimental correlation of the normalized output voltage of demodulation channel and the center wavelength of FBG. Combined with analysis on system demodulation sensitivity, the variation range of λ_s with temperature range of 25∼35° is taken as the system demodulation range, the correlation of the normalized output voltage of demodulation channel and the center wavelength of FBG is fitted with linear function to obtain the short and thick curve shown in Fig. 7, with fitting coefficient of 0.9979. The system normalized sensitivity measured with fitting curve is 5.168/nm, with demodulation range of 0.12 nm.

In Fig. 8, when sensing FBG locates in the middle of two matching FBGs, U' is the least, when sensing FBG has temperature drift, it increases, which is completely consistent to the results of simulation. Since the output power of couplers in system and the FBGs of two sensor channels are impossibly consistent, the maximum output voltage at two ends of demodulation range is not equal. In order to prevent distortion of the vibration signals demodulated, smaller values at ends of demodulation range shall be selected as threshold voltage to determine temperature compensation, and in this Article, such threshold voltage is 0.8905.

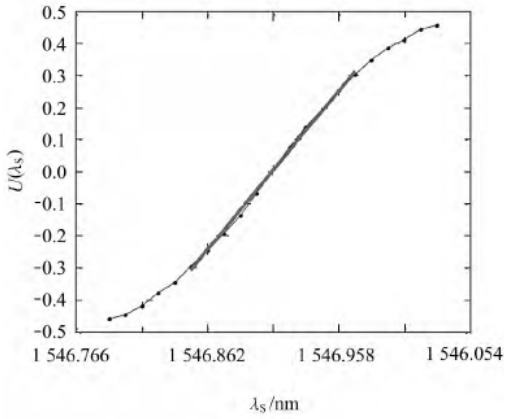

Fig. 7. Measured demodulation channel output voltage versus center wavelength of sensing FBG

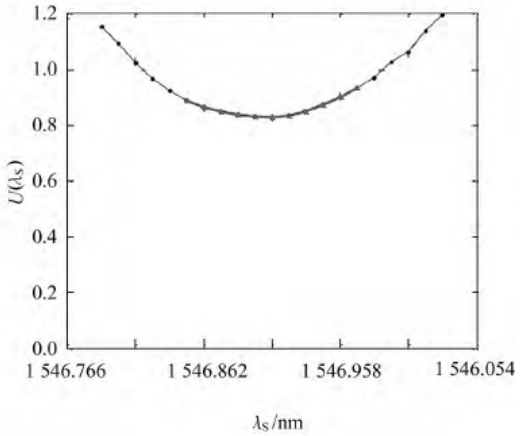

Fig. 8. Measured judging channel output voltage versus center wavelength of sensing FBG

4.3. Vibration test

During experiment, set output vibration signal frequency of vibration table as $f = 60\text{Hz}$, acceleration as $a = 10\text{m}/\text{s}^2$, set TEC controller and make the matching bragg temperature of 30°C; as limited by experimental conditions, regulate ambient temperature near the sensor by indoor air conditioning. Collect and record the output voltage of each channel at 30.0∼28.1 and 22. 8°; remain T_0 at 22. 8 ° and regulate TEC controlling temperature to 22.8°, then collect and record the output voltage of each channel. Results of the 4 groups are shown in Fig. 9, in which the vibration signal cycle is t=1/f o.

We can see from Fig. 9(a) that, when the temperature of sensing FBG is identical to matching FBG and there is no vibration signal, sensing FBG locates in middle of the two matching sensing FBGs. Therefore, the signal measured after vibration signal imposed on sensor essentially has no DC component, with signal frequency of 60Hz, vibration amplitude of 0.0125; and the temperature compensation judging waveform in channel is flat and smooth, with average within 3.0t of 0.8353.

We can see from Fig. 9(b) that, when T_0 is 28.1°, the demodulation waveform is consistent with that in Fig. 9(a), with demodulation waveform frequency of 60 Hz and vibration amplitude of 0.012 3, with error of only 1.44% as compared with Fig. 9(a). But the waveform has DC voltage component, which is caused by temperature drift of sensing FBG. Since temperature drift is minor, the vibration signal achieved by demodulation is barely affected. Meanwhile, the temperature compensation judging waveform in channel is flat and smooth, with average within 3.0t of 0. 8531.

We can see from Fig. 9(c) that, when T_0 changes to 22.8°, the demodulation signal frequency is 60Hz, with amplitude of 0.0106 and variation up to 15.00% as compared with Fig. 9(a). Meanwhile, the average within 3.0t of temperature compensation judging channel waveform is 0.8933, in which waveform has cyclical variation, reflecting from another hand that, the sensing FBG and matching FBG have no normal matching and exceed judging threshold. To this regard, T_{TEC} needs to be changed to reduce the normalized output voltage of the temperature compensation judging channel back to within threshold to prevent distortion of the signals demodulated.

We can see from Fig. 9(d) that, at this moment, the temperature of sensing FBG and matching FBG become the same; the measurements shall be theoretically the same with Fig. 9(a); however, due to regulation errors of T_0, there is slight DC drift in demodulation signal, without impact on the demodulation results. Meanwhile, the demodulation waveform frequency is 60 Hz, with amplitude of 0.1240 and error of only 0.6% as compared with Fig. 9(a). The temperature compensation judging waveform in channel is flat and smooth, with average within 3.0t of 0.836.

5. Conclusion

A double-matching FBG vibration demodulation system with function of temperature compensation is designed in this Article for simulation and analysis of

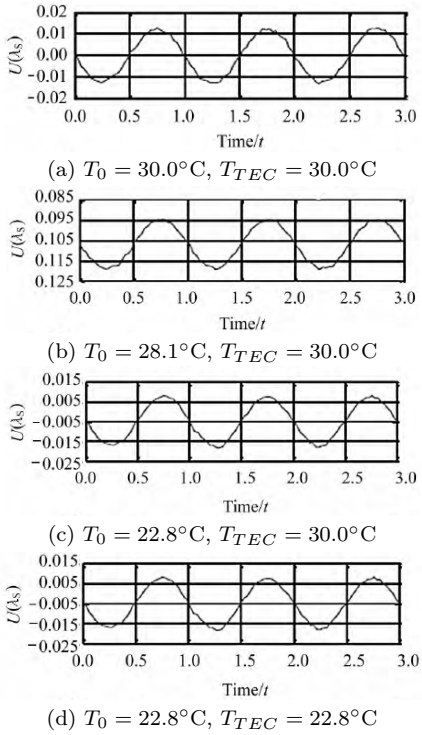

Fig. 9. Waveforms four different groups of T_0 and TFC control temperatures

the performance of system demodulation, the results show that, the transmissive double-matching FBG method can promote system demodulation sensitivity and demodulation range significantly. Meanwhile, system temperature compensation is achieved effectively by the matching of center wavelengths of matching FBG and sensing FBG with TEC controlling the matching FBG sealing ambient temperature.

The results of experiment show that, the demodulation sensitivity of double-matching FBG vibration demodulation system designed in this paper is 5.168/nm, with demodulation range of 1.2 nm, normalized threshold voltage of temperature compensation judging channel is 0.8905. The temperature compensation method can address the effect of temperature drift on FBG based vibration demodulation system effectively, with certain practical value.

References

[1] K. Kato, J. Sato: *Vibration-type angular velocity detector having sensorless temperature compensation: US*, US 5806364 A[P], (1998).

[2] Y. Ren, D. Xu, F. L. Qin: *A Method for Vibration-Cylinder Air-Pressure Sensor Temperature Compensation Based on Radial Basis Function (RBF) Neural Network*[J]. Applied Mechanics & Materials, *236-237* (2012), 1232–1237.

[3] T. Li, C. Shi, Y. Tan, et al.: *A diaphragm type fiber Bragg grating vibration sensor*

based on transverse property of optical fiber with temperature compensation[J]. IEEE Sensors Journal, (2017), No. 99, 1-1.

[4] T. Li, Y. Tan, Z. Zhou Z., et al.: *A non-contact FBG vibration sensor with double differential temperature compensation*[J]. Optical Review, *23* (2016), No. 1, 26–32.

[5] S. Janssen, K. Schmitt, M. Blanke, et al.: (2014) *Ethylene detection in fruit supply chains.*[J]. Philos Trans A Math Phys Eng Sci, *372*(2017), 20130311.

[6] W. Xu, W. Wu, F. Zhen, et al.: *Temperature Drift Compensation for Hemispherical Resonator Gyro Based on Natural Frequency*[J]. Sensors, *12* (2012), No. 5, 6434–46.

[7] B. Yu: *Design of Oil Mist Detector Based on Light Scattering*[J]. Optics & Optoelectronic Technology, *7* (2009), No. 1, 62–65.

[8] J. Yu, J. Li, Q. Dai, et al.: *Temperature Compensation and Data Fusion Based on a Multifunctional Gas Detector*[J]. IEEE Transactions on Instrumentation & Measurement, *64* (2014), No. 1, 204–211.

[9] E. Eryurek: *Device in a process system for validating a control signal from a field device: WO*, US 6047220 A[P], (2000).

[10] M. Rhimi, N. Lajnef, N. Lajnef: *Passive temperature compensation in piezoelectric vibrators using shape memory alloy-induced axial loading.* J. Intell. Mater. Syst. Struct. *23* (2012), No. 15, 1759–1770[.

[11] T. Li, Y. Tan, X. Han, et al.: *Diaphragm Based Fiber Bragg Grating Acceleration Sensor with Temperature Compensation*[J]. Sensors, *17* (2017), No. 1, 218.

[12] F. Ju, X. Ma, T. Liu: *Temperature Compensation in DFB Laser Vibration Interrogating System*[J]. Semiconductor Technology, *35* (2010), No. 8, 823–826.

Received May 7, 2017